Supporting Information

Two solvent-dependent Al_{16} nanorings: design synthesis and nonlinear optical limiting behavior

San-Tai Wang, ‡[a,b] Xiao Qi, ‡[a,b] Ran-Qi Chen, [a] Wei-Hui Fang *[a] and Jian Zhang *[a]

[a]State Key Laboratory of Structural Chemistry, Fujian Institute of Research on the Structure of Matter, Chinese Academy of Sciences, Fuzhou, Fujian 350002, P.R. China.
[b]University of Chinese Academy of Sciences, Bejing, 100049, P.R. China.
Email: fwh@fjirsm.ac.cn
‡These authors contributed equally.

Table of content

Materials and Instrumentation

All the reagents and solvents employed were purchased commercially and used as received without further treatment. Aluminum isopropoxide ($Al(O^iPr)_3$) was purchased from Aladdin Chemical Reagent Shanghai, while 2-naphthoic acid was purchased from Adamas-beta. Hexamethylene tetramine, phenol (≥99.0%), 1-propanol (≥99.5%), 1, 4-dioxane (≥99.5%), methylamine solution in alcohol (27%~32%) and N, N-dimethylformamide (DMF) (≥99.5%) were acquired from Sinopharm Chemical Reagent Beijing.

After fully grinding the crystals, they were made into transparent round slices in a fully automatic tablet press for testing. The **Fourier transform infrared spectroscopy (FT-IR)** data were collected on a PerkinElmer Spectrum 100 FT-IR Spectrometer over a range 400-4000 cm^{-1}.

Single crystal samples of **AlOC-134** to **AlOC-135** were grinded in a mortar and sieved with a 200 molybdenum sieve and then used for testing. The **powder X-ray diffraction (PXRD)** data were collected on a Rigaku Mini Flex II diffractometer using Cu-Kα radiation (λ = 1.54056 Å) under ambient conditions. Molecular modeling was carried out using Reflex Plus, a module implemented in Materials Studio (version 4.4) by Accelrys Inc. The initial structures were constructed piecewise starting with a monoclinic cell with space group *C*2/c for **AlOC-134**, and a tetragonal cell with space group $P4_2/n$ for **AlOC-135**. For **AlOC-134** and **AlOC-135**, the Tomandl Pseudo-Voigt function was used for whole profile fitting and the Berrar-Baldinozzi function was used for asymmetry correction during the refinement processes.

The **UV-vis diffuse reflection** data were recorded at room temperature using a powder sample with $BaSO_4$ as a standard (100% reflectance) on a PerkinElmer Lamda-950 UV spectrophotometer and scanned at 200-800 nm. The absorption data are calculated from the Kubelka-Munk function, ($F(R) = (1-R)^2/2R$), where R representing the reflectance.

The **thermogravimetric analyses (TGA)** were performed on a Mettler Toledo TGA/SDTA 851e analyzer in a nitrogen atmosphere with a heating rate of 10 ^oC/min.

The **energy dispersive spectroscopy (EDS)** analyses of single cleaned crystal were performed on a JEOL JSM6700F field-emission scanning electron microscope equipped with an Oxford INCA system.

Supporting Figures

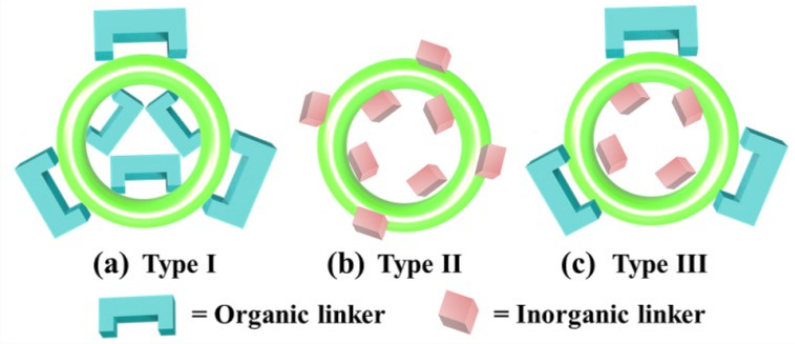

Scheme S1 Three connection types in cyclic compounds.

The Structure of AlOC-134 and AlOC-135 Rings

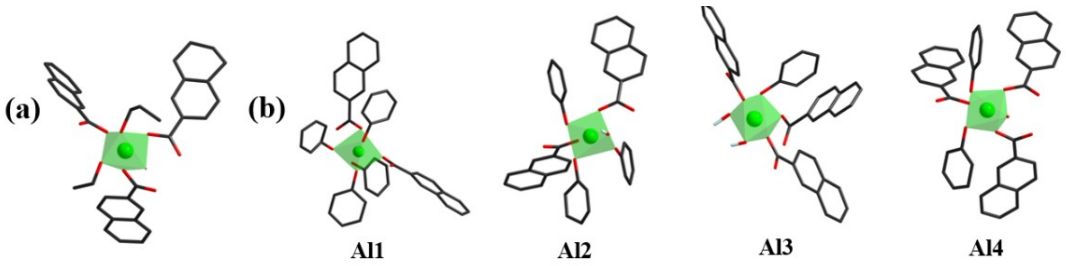

Figure S1 Coordination environment of Al^{3+} ions in **AlOC-134** (a) and **AlOC-135** (b). Color code: Al, green; O, red; C, black.

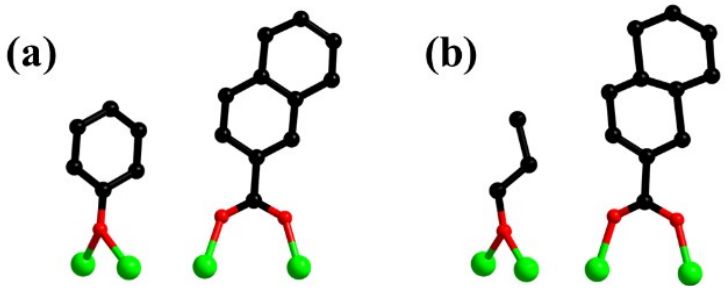

Figure S2 Ligand coordination mode of **AlOC-134** (a) and **AlOC-135** (b). Color code: Al, green; O, red; C, black.

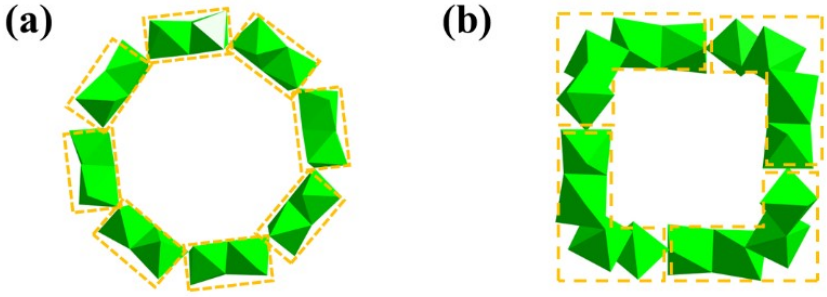

Figure S3 Connection mode of Al_2 dimers (a) and Al_4 dimers (b) through vertex sharing mode.

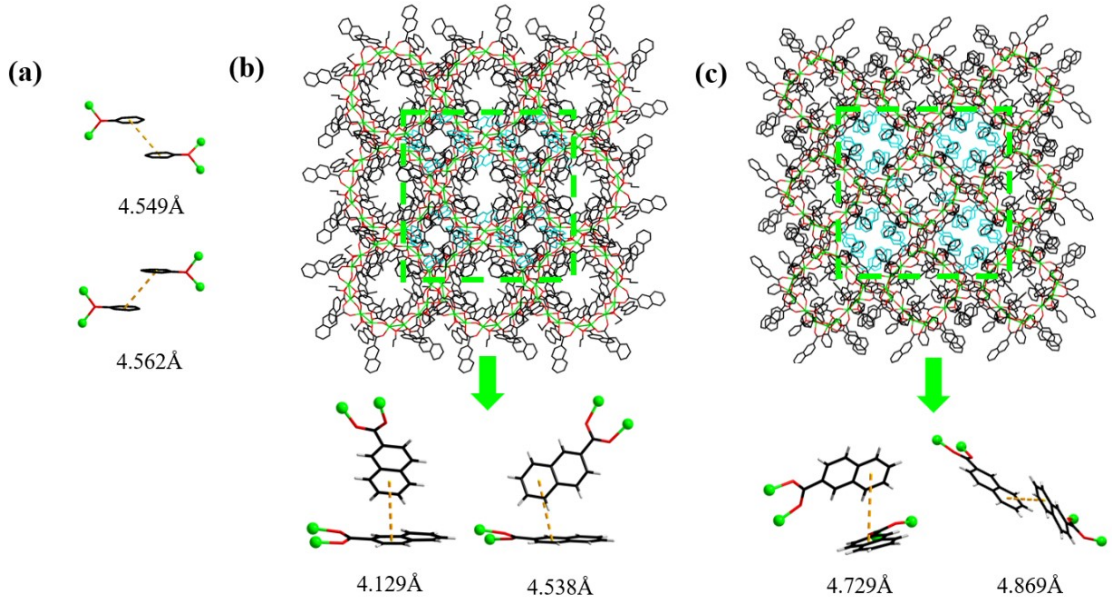

Figure S4 (a) The intramolecular π···π stacking interaction of **AlOC-135**. (b) The intermolecular π···π stacking interaction of **AlOC-134**. (c) The intermolecular π···π stacking interaction of **AlOC-135**. Color code: Al, green; O, red; C, black; C with π···π stacking interaction, blue.

Series Characterization of AlOC-134 and AlOC-135 Molecular Rings

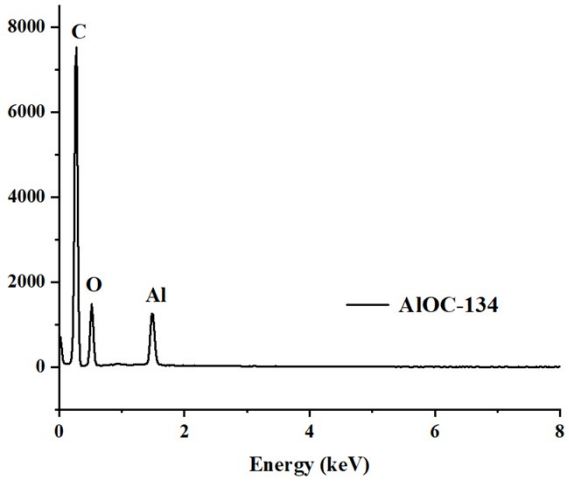

Figure S5 The EDS spectrum of compound **AlOC-134**.

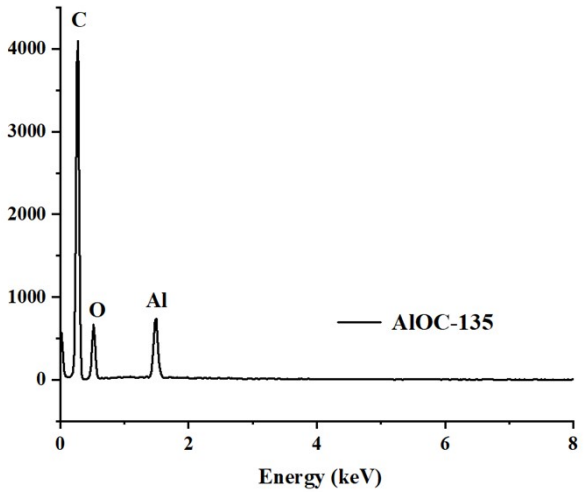

Figure S6 The EDS spectrum of compound **AlOC-135**.

Discussion for EDS spectra: The elemental composition of **AlOC-134** and **AlOC-135** can be obtained from the EDS spectrum (Al, C and O), in which show similar proportions of elements.

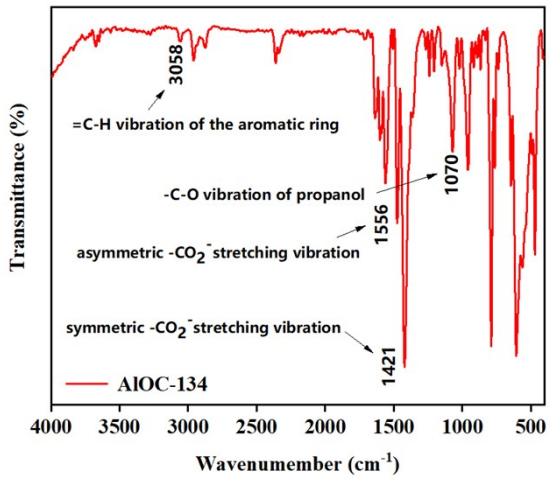

Figure S7 FT-IR spectra of **AlOC-134**.

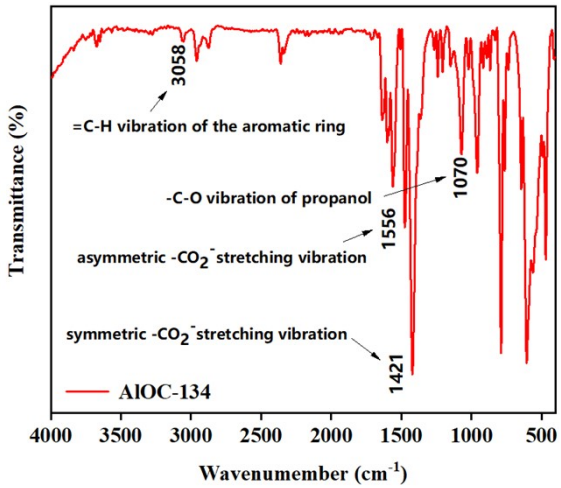

Figure S8 FT-IR spectra of **AlOC-135**.

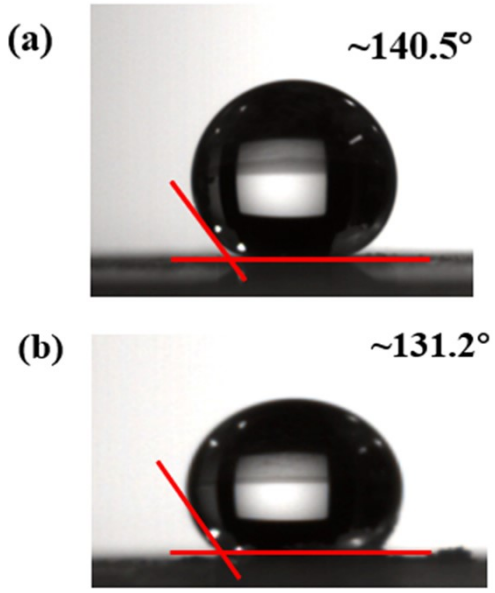

Figure S9 The contact angles of water droplet of **AlOC-134** (a) and **AlOC-135** (b).

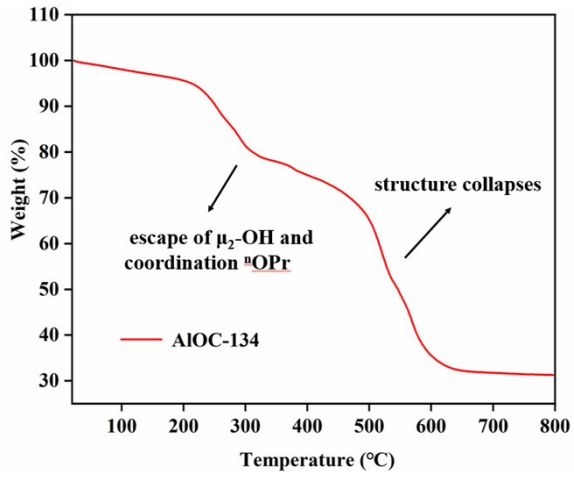

Figure S10 The TGA plot of **AlOC-134**.

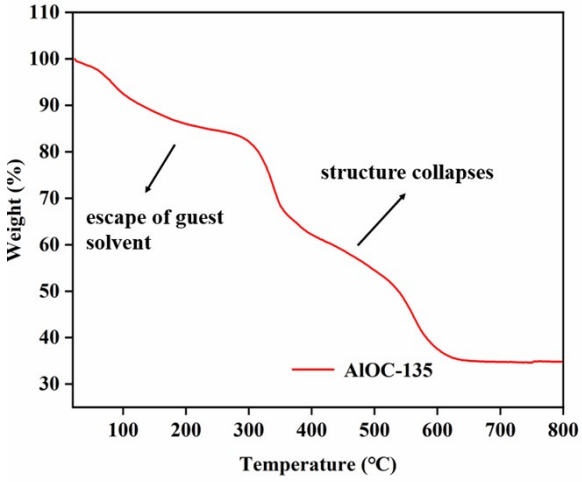

Figure S11 The TGA plot of **AlOC-135**.

Discussion for TGA curve: The thermal stability of **AlOC-134** and **AlOC-135** was investigated in N_2 atmosphere up to 800 °C with a heating rate of 10 K min^{-1}. The thermal stability of the two compounds is slightly different. For **AlOC-134**, the first stage of weightlessness may be due to the escape of μ_2-OH and the coordination ^{n}OPr, further collapses when the temperature is heated to 500 °C. For **AlOC-135**, the early thermogravimetric loss may be caused by the escape of guest solvents. At 600 °C, the two compounds completely collapse into Al_2O_3.

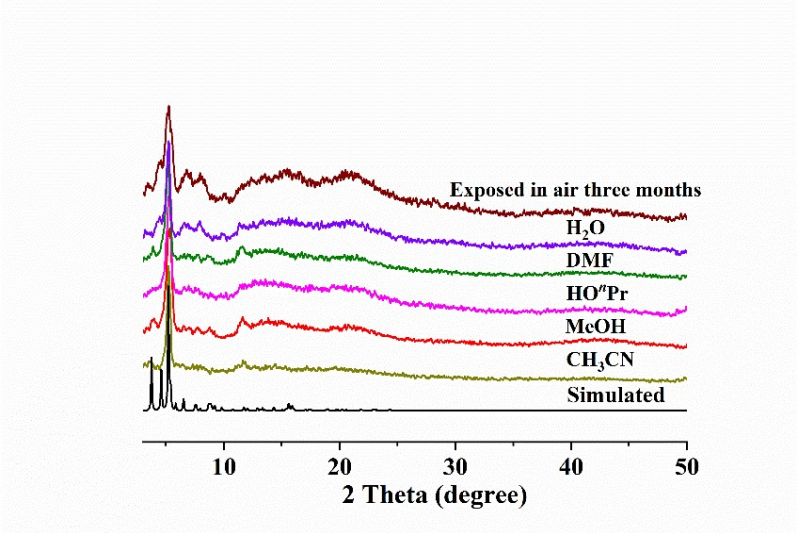

Figure S12 The PXRD patterns of **AlOC-134** in different organic solvents at room temperature for 24 hours.

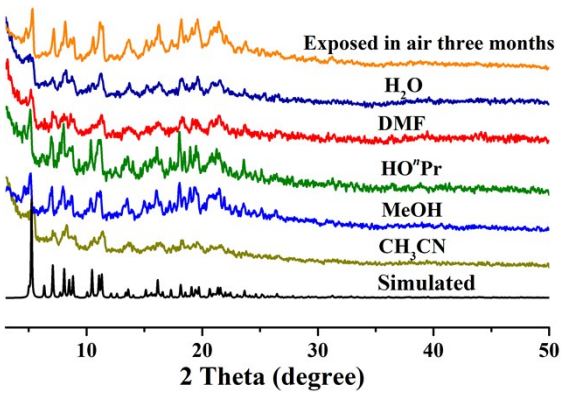

Figure S13 The PXRD patterns of **AlOC-135** in different organic solvents at room temperature for 24 hours.

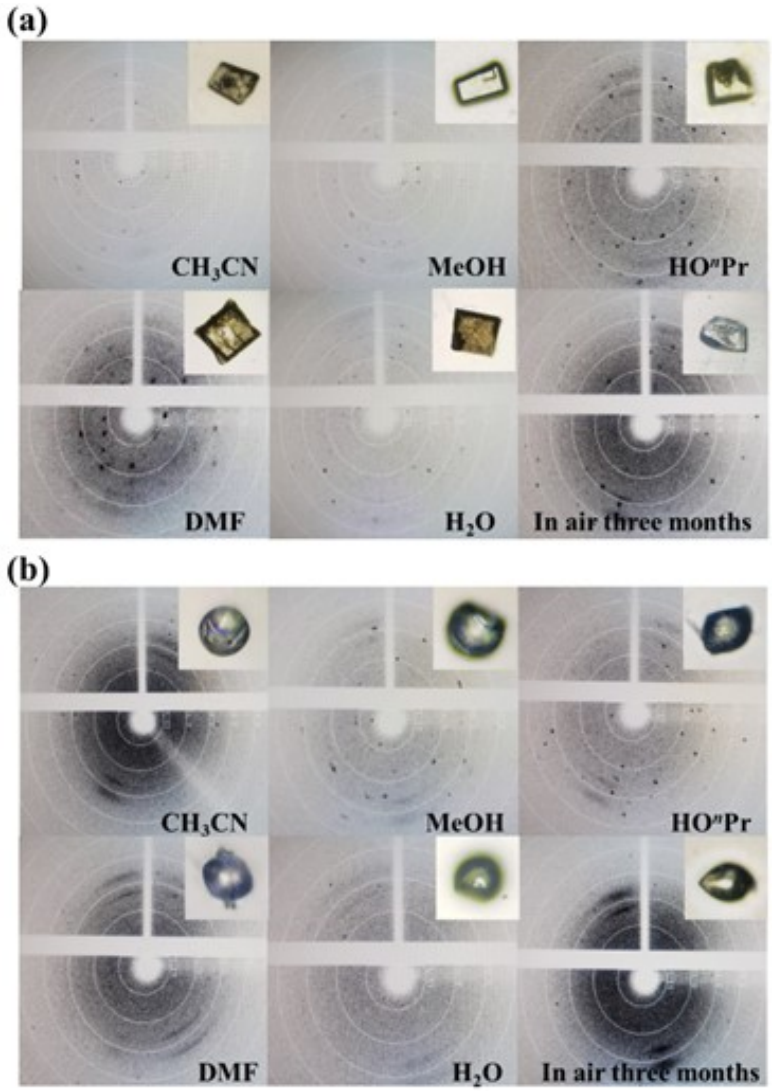

Figure S14 The diffraction images of **AlOC-134** (a) and **AlOC-135** (b) were placed in air for 3 months and soaked in solvent for 3 days (insert is the corresponding single crystal morphology).

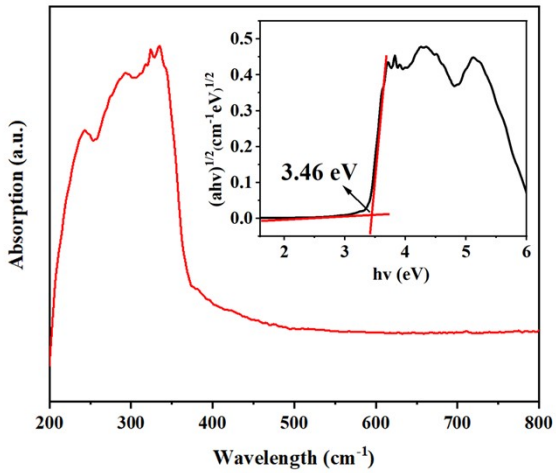

Figure S15 The UV-vis diffuse reflectance spectra of **AlOC-134** (inset is the band gap).

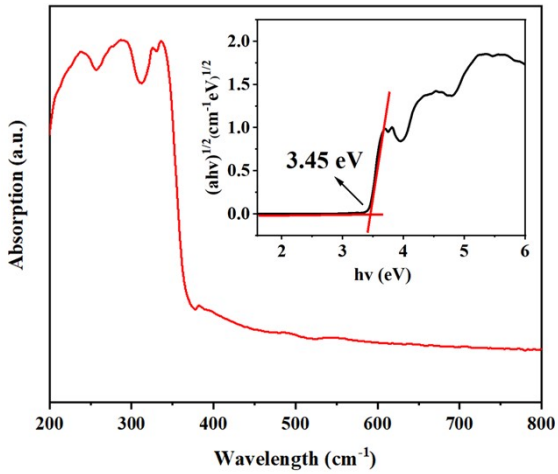

Figure S16 The UV-vis diffuse reflectance spectra of **AlOC-135** (inset is the band gap).

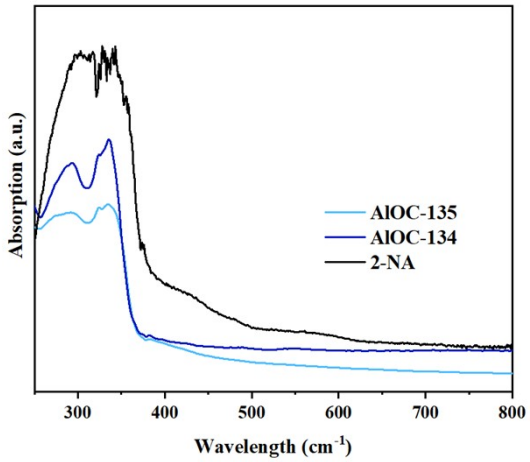

Figure S17 The UV-vis diffuse reflectance spectra of **AlOC-134**, **AlOC-135** and 2-NA. The absorption peaks of **AlOC-134** and **AlOC-135** are slightly red-shifted compared to the 2-NA ligands.

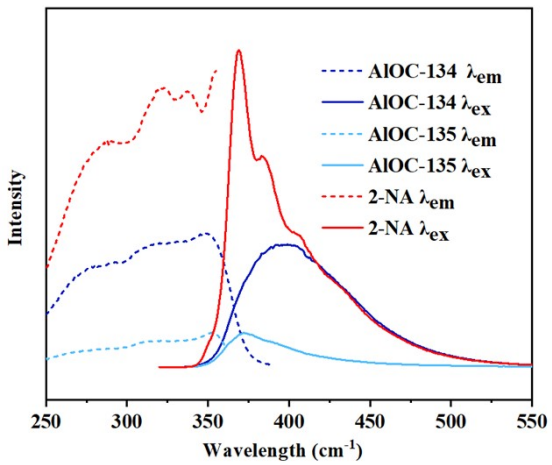

Figure S18 Room-temperature photoluminescence spectra of **AlOC-134**, **AlOC-135** and 2-NA (λ_{em} is measured under excitation with λ_{ex}=300 nm).

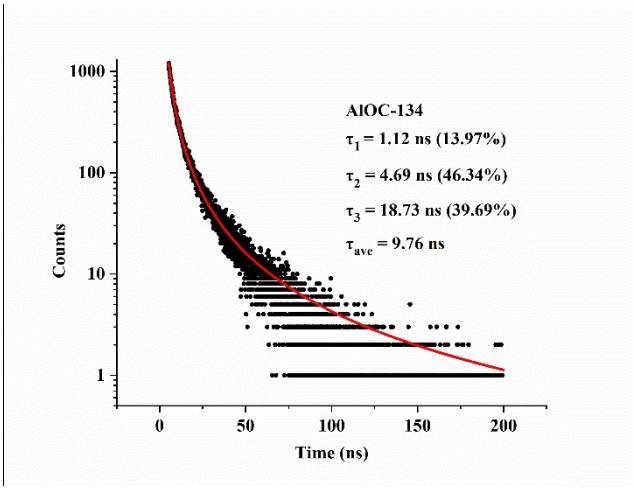

Figure S19 The time-resolved PL decay curve **AlOC-134**.

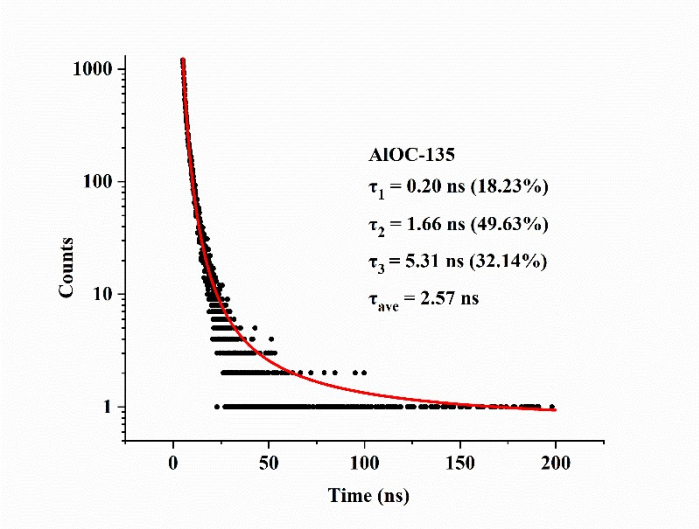

Figure S20 The time-resolved PL decay curve **AlOC-135**.

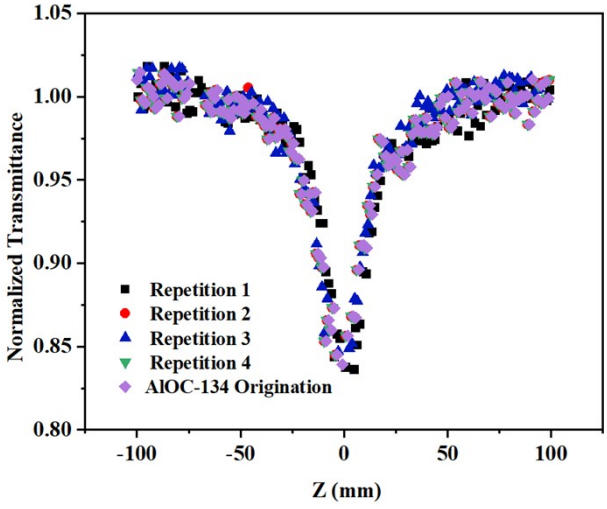

Figure S21 The repeatability of third-order NLO responses for **AlOC-134**.

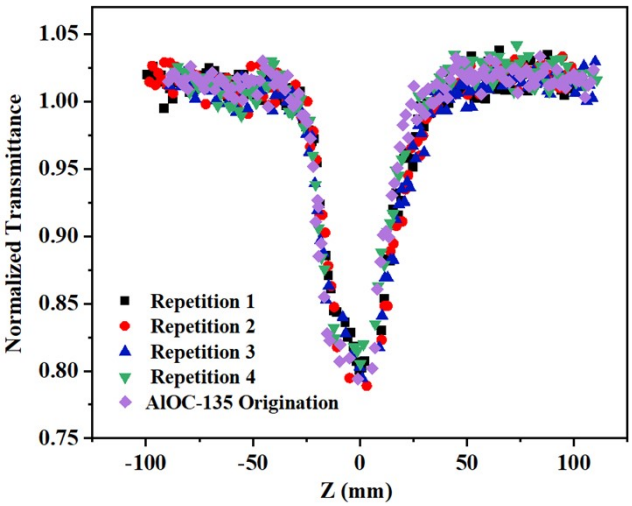

Figure S22 The repeatability of third-order NLO responses for **AlOC-135**.

Supporting Tables

Crystallographic Data

Table S1 Crystallographic data and structural refinements.

Identification code	**AlOC-134**	**AlOC-135**
CCDC Nos.	2289659	2289660
Empirical formula	$C_{312}H_{288}Al_{16}O_{72}$	$C_{340}H_{248}Al_{16}O_{68}$
Formula weight	5621.09	14188.3(4)
Temperature/K	300	293
Crystal system	monoclinic	tetragonal
Space group	*C*2/c	$P4_2/n$
a /Å	33.3623(8)	24.8708(2)
b /Å	34.9963(9)	24.8708(2)
c /Å	34.0895(9)	22.9377(6)
α /°	90	90(3)
β /°	90.857(2)	90(3)
γ /°	90	90(3)
V olume/Å^3	39797.0(18)	14184.3(4)
Z	4	2
ρ_{calc} g/cm^{-3}	0.938	1.370
μ /mm^{-1}	0.552	0.786
F(000)	117766.0	6080.0
Radiation	GaKα(λ=1.3405)	GaKα(λ=1.3405)
2θ range for data collection/°	4.256 to 120.078	4.376 to 102.090
Reflections collected	81140	116377
Independent reflections	40012[R_{int}=0.0446, R_{sigema}=0.0602]	40012[R_{int}=0.0866, R_{sigema}=0.0449]
Data/restraints/parameters	40012/187/1760	16286/144/958
Goodness-of-fit on F^2	1.105	1.169
Final R indexes [I>2σ(I)]	R_1 = 0.0986 wR_2 = 0.3331	R_1 = 0.0.0978 wR_2 = 0.3386
Final R indexes [all data]	R_1 = 0.1201 wR_2 = 0.3546	R_1 = 0.1568 wR_2 = 0.3524
Largest diff. peak/hole /e Å^{-3}	1.051/-0.501	0.942/-0.590

Bond Lengths of AlOC-134 and AlOC-135

Table S2 Bond lengths [Å] for **AlOC-134** and **AlOC-135**.

Bond lengths [Å] for **AlOC-134**							
Al01-O09	1.862(3)	Al02-O0C	1.880(2)	Al03-O09	1.847(3)	Al04-O0B	1.875(3)
Al01-O0C	1.875(3)	Al02-O0F	1.913(3)	Al03-O0A	1.853(3)	Al04-O0D	1.865(3)
Al01-O0E	1.882(3)	Al02-O0G	1.901(3)	Al03-O0J	1.873(3)	Al04-O0H	1.855(3)
Al01-O0K	1.915(3)	Al02-O0M	1.945(3)	Al03-O0X	1.946(3)	Al04-O0S	1.888(3)
Al01-O0N	1.907(3)	Al02-O0P	1.859(3)	Al03-O0Z	1.898(3)	Al04-O0Y	1.947(3)
Al01-O0P	1.872(3)	Al02-O0Q	1.853(3)	Al03-O10	1.927(3)	Al04-O11	1.929(3)
Al05-O0H	1.860(3)	Al06-O0I	1.867(3)	Al07-O0B	1.883(3)	Al08-O0A	1.868(3)
Al05-O0I	1.865(3)	Al06-O0L	1.875(3)	Al07-O0D	1.872(3)	Al08-O0J	1.873(3)
Al05-O0L	1.884(3)	Al06-O0O	1.895(3)	Al07-O0Q	1.855(3)	Al08-O0U	1.863(3)
Al05-O0T	1.885(3)	Al06-O0U	1.844(3)	Al07-O0R	1.886(3)	Al08-O0V	1.898(3)
Al05-O0W	1.913(3)	Al06-O12	1.912(3)	Al07-O015	1.924(3)	Al08-O014	1.913(3)
Al01-O005	1.884(2)	Al02-O005	1.890(3)	Al03-O007	1.841(3)	Al04-O008	1.902(3)
Bond lengths [Å] for **AlOC-135**							
Al01-O006	1.923(3)	Al02-O006	1.910(3)	Al03-O009	1.955(3)	Al04-O00D	1.838(3)
Al01-O008	1.913(3)	Al02-O007	1.864(3)	Al03-O00D	1.840(3)	Al04-O00E	1.909(3)
Al01-O00A	1.908(3)	Al02-O009	1.913(3)	Al03-O00F	1.904(3)	Al04-O00J	1.909(4)
Al01-O00C	1.897(4)	Al02-O00B	1.899(3)	Al03-O00G	1.935(3)	Al04-O00K	1.853(3)
Al01-O00E	1.891(3)	Al02-O00H	1.898(3)	Al03-O00I	1.895(3)	Al04-O00L	1.890(3)

Supramolecular Force Table Statistics

Table S3 Hydrogen bond parameters for **AlOC-134**.

D-H···A	d(D-H)	d(H···A)	d(D···A)	∠(DHA)
C01M-H01M···O00I	0.95	2.43	2.758(6)	100
C01S-H01S···O00Q	0.95	2.47	2.785(7)	100
C01X-H01X···O00N	0.95	2.43	2.756(7)	100
C02A-H02A···O00N	0.99	2.44	3.059(8)	120
C02A-H02B···O00Y	0.99	2.58	2.919(7)	100
C02O-H02O···O014	0.95	2.42	2.739(8)	100
C02V-H02V···O00M	0.95	2.36	2.691(8)	100
C034-H03A···O00Y	0.99	2.55	3.175(8)	121
C039-H039···O018	0.95	2.46	2.779(9)	100
C03G-H03K···O00J	0.95	2.42	2.772(8)	102
C03M-H03R···O0F	0.99	2.45	3.041(11)	118
C03M-H03S···O014	0.99	2.47	2.980(11)	112
C03P-H03V···O013	0.99	2.37	2.994(8)	120
C04D-H04I···O00J	0.99	2.49	3.110(11)	120
C04F-H04K···O00S	0.99	2.4	2.948(11)	114

C04F-H04L···O017	0.99	2.48	3.078(13)	118
C04R-H04Z···O0D	0.99	2.58	3.288(13)	129
C04W-H6AA···O00P	0.95	2.43	3.335(15)	159

Table S4 Hydrogen bond parameters for **AlOC-135**.

D-H···A	d(D-H)	d(H···A)	d(D···A)	∠(DHA)
C00U-H00U···O00K	0.93	2.41	2.831(6)	100
C018-H18···O00J	0.93	2.4	2.721(7)	100

Table S5 The π…π interaction of **AlOC-134** and **AlOC-135**.

The π…π interaction of **AlOC-134**		
Aromatic ring A	Aromatic ring B	Distance between A-B ring centroids (Å)
intermolecular π-π interaction		
C02C, C035, C047, C0AA, C05M, C05G	C028, C02L, C02Q, C02Y, C039, C03X	4.13
C04N, C021, C05E, C02X, C03V, C03J	C03N, C04B, C04K, C05B, C04L, C04W	4.54
The π…π interaction of **AlOC-135**		
Aromatic ring A	Aromatic ring B	Distance between A-B ring centroids (Å)
Intramolecular π-π interaction		
C00T(#5), C017(#6), C01L(#7), C01E(#8), C002(#9), C01N(#10)	C00T(#11), C017(#12), C01L(#13), C01E(#14), C002(#15), C01N(#16)	4.56
C00T(#5), C017(#6), C01L(#7), C01E(#9), C002(#10), C01N(#13)	C00T(#8), C017(#11), C01L(#12), C01E(#14), C002(#15), C01N(#16)	4.55
Intermolecular π-π interaction		
C6, C12, C01Z, C02Y, C02W, C01X	C00V, C018, C01C, C01G, C01H, C01K	4.73
C014, C02N, C02B, C02G, C02X, C02R	C6, C12, C01Z, C02Y, C02W, C01X	4.87

BVS Analysis

Table S6 BVS analysis for **AlOC-134**.

BVS Value	Bond distances		BVS Value	Bond distances	
Al01 3.1819	Al01-O09	1.862(3)	Al02 3.1363	Al02-O0C	1.880(2)
	Al01-O0C	1.875(3)		Al02-O0F	1.913(3)
	Al01-O0E	1.882(3)		Al02-O0G	1.901(3)
	Al01-O0K	1.915(3)		Al02-O0M	1.945(3)
	Al01-O0N	1.907(3)		Al02-O0P	1.859(3)
	Al01-O0P	1.872(3)		Al02-O0Q	1.853(3)
BVS Value	Bond distances		BVS Value	Bond distances	
Al03 3.1595	Al03-O09	1.847(3)	Al04 3.1265	Al04-O0B	1.875(3)
	Al03-O0A	1.853(3)		Al04-O0D	1.865(3)
	Al03-O0J	1.873(3)		Al04-O0H	1.855(3)
	Al03-O0X	1.946(3)		Al04-O0S	1.888(3)
	Al03-O0Z	1.898(3)		Al04-O0Y	1.947(3)
	Al03-O10	1.927(3)		Al04-O11	1.929(3)
BVS Value	Bond distances		BVS Value	Bond distances	
Al05 3.2078	Al05-O0H	1.860(3)	Al06 3.1501	Al06-O0I	1.867(3)
	Al05-O0I	1.865(3)		Al06-O0L	1.875(3)
	Al05-O0L	1.884(3)		Al06-O0O	1.895(3)
	Al05-O0T	1.885(3)		Al06-O0U	1.844(3)
	Al05-O0W	1.913(3)		Al06-O12	1.912(3)
	Al05-O017	1.887(3)		Al06-O013	1.949(3)
BVS Value	Bond distances		BVS Value	Bond distances	
Al07 3.1787	Al07-O0B	1.883(3)	Al08 3.2065	Al08-O0A	1.868(3)
	Al07-O0D	1.872(3)		Al08-O0J	1.873(3)
	Al07-O0Q	1.855(3)		Al08-O0U	1.863(3)
	Al07-O0R	1.886(3)		Al08-O0V	1.898(3)
	Al07-O015	1.924(3)		Al08-O014	1.913(3)
	Al07-O016	1.896(3)		Al08-O018	1.880(3)

Bond valence = exp((Ro-R)/B), where Ro values for Al-O bond length is 1.644, B is 0.38. The (μ_2-OH) are O0E, O0D, O00Z and O00L.

Table S7 BVS analysis for **AlOC-135**.

BVS Value	Bond distances		BVS Value	Bond distances	
Al01 3.0394	Al01-O005	1.884(2)	Al02 3.0969	Al02-O005	1.890(3)
	Al01-O006	1.923(3)		Al02-O006	1.910(3)
	Al01-O008	1.913(3)		Al02-O007	1.864(3)
	Al01-O00A	1.908(3)		Al02-O009	1.913(3)
	Al01-O00C	1.897(4)		Al02-O00B	1.899(3)
	Al01-O00E	1.891(3)		Al02-O00H	1.898(3)
BVS Value	Bond distances		BVS Value	Bond distances	
Al03 3.1197	Al03-O007	1.841(3)	Al04 3.2035	Al04-O008	1.902(3)
	Al03-O009	1.955(3)		Al04-O00D	1.838(3)
	Al03-O00D	1.840(3)		Al04-O00E	1.909(3)
	Al03-O00F	1.904(3)		Al04-O00J	1.909(4)
	Al03-O00G	1.935(3)		Al04-O00K	1.853(3)
	Al03-O00I	1.895(3)		Al04-O00L	1.890(3)

Bond valence = exp((Ro-R)/B), where Ro values for Al-O bond length is 1.644, B is 0.38. The (μ_2-OH) are O00D and O007.

Sample (AlOCs@PDMS) Information and Third-order Test Parameters

Table S8 Sample information and nonlinear optics parameters.

Sample	**AlOC-134**	**AlOC-135**
Linear transmittance	0.50	0.51
Thickness (mm)	1.05	0.74
OL threshold[a] (J/cm^2)	3.98	0.62
Nonlinear transmittance	0.84	0.79
β[b] (cm/GW)	22	41
α[c] (cm^{-1})	6.60	9.10
Im $\chi^{(3)}$ [d] (10^{-12} esu)	4.65	8.66
FOM[e] (10^{-12} esu)	0.70	0.95

[a] OL threshold is defined as the input fluency at which the transmittance is 50% of the linear transmittance; [b] β is the nonlinear absorption coefficient; [c] α being the linear absorption coefficient at the laser wavelength; [d] Im $\chi^{(3)}$ is third-order susceptibility $\chi^{(3)}$ values; [e] FOM is the ratio of third-order susceptibility $\chi^{(3)}$ and linear absorption coefficient at the laser wavelength.

Supplement of Representative NLO Material

Table S9 Comparison of Nonlinear Optics Parameters.

Compounds	Text Condition	α[a] (cm^{-1})	β[b] (cm/GW)	OL threshold[c] (J/cm^2)	Ref.
Pt-Ni NP/reduced graphene oxide	in C_2H_5OH	-	1.64	2.49 (in gel glass)	1
Pt-Ni cluster/reduced graphene oxide	in C_2H_5OH	-	1.98	1.42 (in gel glass)	1
$[(n\text{BuSn})_{12}(OH)_{23}O(AgO_4)]_2 \cdot 6(Ac) \cdot 2(PCA) \cdot 7CH_3CN$ (Bu = butylgroup; HAc = aceticacid; HPCA = 2-pyrazinecarboxylic acid)	KBr pellet	-	2.55	0.50	2
graphene oxide	in DMF	5.13	6.19	-	3
$(Tp^*WS_3Cu_3)_4(\mu_4\text{-}S)_4(Ag)]OTf \cdot 0.33CHCl_3$ ($OTf = CF_3SO_3$)	PVBC film	-	18.00	-	4
$(Al_{16}(^n OPr)_{16}(\mu_2\text{-}OH)_8(2\text{-}NA)_{24})$ ($^n OPr$ = n-propanol, 2-NA = 2-naphthoic acid)	PDMS film	6.60	22.00	3.98	This work
$[Tp^*WS_3Cu_2(L^a)]_6(OTf)_6$ (Tp* = hydridotris(3,5-dimethylpyrazol-1-yl)borate), L^a = 1,4-di(pyridin-4-yl)-buta-1,3-diyne, $OTf = CF_3SO_3$)	PVA film	-	26.00	-	5
zinc phthalocyanine	in DMF	6.24	31.07	-	3
$(Al_{16}(phenol)_{20}(\mu_2\text{-}OH)_8(2\text{-}NA)_{20})$ (2-NA = 2-naphthoic acid)	PDMS film	9.10	41.00	0.62	This work
$[(Tp^*WS_3Cu_3)_2(Tp^*_2W_2Cu_3S_7)_3](PF_6)$	PVBC film	-	45.00	-	4
detonation nanodiamonds-2,9(10),16(17),23(24)-tetrakis-(4-pyridyloxy) phthalocyaninato	in DMSO	17.95	58.50	-	6
single-walled carbon nanotube-5,10,15,20-tetraphenylporphyrin	in DMF	-	105.00	-	7
detonation nanodiamonds- phthalocyanato silicon (IV) hydroxide	in DMSO	1.73	125.00	0.47	6
reduced graphene oxide	PMMA film	24.59	129.01	-	8
phthalocyanato silicon (IV) hydroxide	in DMSO	2.59	136.00	0.39	6
poly[(9,9-dihexyl-9H-fluorene)-alt-(1,1,2,2-tetraphenylethene)]- reduced graphene oxide	PMMA film	12.19	215.77	-	8
$[Zn_3(TPyP)(H_2O)_2(C_2O_4)_2]$ ($TPyP(H_2)$ = 5,10,15,20-tetra(4-pyridyl)porphyrin)	PDMS film	-	400.00	0.57	9

$[Zn_2(TPyP)(AC)_2]$ (TPyP(H_2) = 5,10,15,20-tetra(4-pyridyl)porphyrin)	PDMS film	-	1350.00	-	9

The compounds are arranged in order of β value. [a] α being the linear absorption coefficient at the laser wavelength; [b] β is the nonlinear absorption coefficient; [c] OL threshold defined as the input fluency at 50% linear transmittance.

References

1 C. Zheng, L. Lei, J. Huang, W. Chen, W. Li, H. Wang, L. Huang and D. Huang, Facile control of metal nanoparticles from isolated nanoparticles to aggregated clusters on two-dimensional graphene to form optical limiters, *J. Mater. Chem. C*, 2017, **5**, 11579–11589.

2 Y. Zhu, Z. Wang, D. Li, Y. Zhu, Q. Li, D. Li and L. Zhang, Silver-Templated γ-Keggin Alkyltin-Oxo Cluster: Electronic Structure and Optical Limiting Effect, *Angew. Chem. Int Ed.*, 2022, **61**, e202202853.

3 J. Zhu, Y. Li, Y. Chen, J. Wang, B. Zhang, J. Zhang and W. J. Blau, Graphene oxide covalently functionalized with zinc phthalocyanine for broadband optical limiting, *Carbon*, 2011, **49**, 1900–1905.

4 Z.-K. Wang, M.-H. Du, P. Braunstein and J.-P. Lang, A Cut-to-Link Strategy for Cubane-Based Heterometallic Sulfide Clusters with Giant Third-Order Nonlinear Optical Response, *J. Am. Chem. Soc.*, 2023, **145**, 9982–9987.

5 S.-J. Bao, Z.-M. Xu, Z.-W. Huang, T.-C. Yu, M.-Y. Wang, Y.-L. Song, Z. Niu, B. F. Abrahams and J.-P. Lang, A hierarchical supramolecular assembly strategy for remarkably amplifying third-order nonlinear optical responses of clusters, *Sci. China Mater.*, 2023, **66**, 3278–3284.

6 R. Matshitse, S. Khene and T. Nyokong, Photophysical and nonlinear optical characteristics of pyridyl substituted phthalocyanine-Detonation nanodiamond conjugated systems in solution, *Diam. Relat. Mater.*, 2019, **94**, 218–232.

7 Z.-B. Liu, J.-G. Tian, Z. Guo, D.-M. Ren, F. Du, J.-Y. Zheng and Y.-S. Chen, Enhanced Optical Limiting Effects in Porphyrin-Covalently Functionalized Single-Walled Carbon Nanotubes, *Adv. Mater.*, 2008, **20**, 511–515.

8 Z. Liu, N. Dong, P. Jiang, K. Wang, J. Wang and Y. Chen, Reduced Graphene Oxide Chemically Modified with Aggregation-Induced Emission Polymer for Solid-State Optical Limiter, *Chem. Eur. J.*, 2018, **24**, 19317–19322.

9 D.-J. Li, Q. Li, Z.-R. Wang, Z.-Z. Ma, Z.-G. Gu and J. Zhang, Interpenetrated Metal-Porphyrinic Framework for Enhanced Nonlinear Optical Limiting, *J. Am. Chem. Soc.*, 2021, **143**, 17162–17169.